Arabidopsis Type I Metacaspases Control Cell Death

Nuria S. Coll, *et al.*

Science **330**, 1393 (2010);
DOI: 10.1126/science.1194980

and *Bid*$^{-/-}$ *Bim*$^{-/-}$*Puma*$^{-/-}$ TKO cells (Fig. 4E and fig. S14).

The lack of strong and stable interaction between BH3s and BAX/BAK was thought to support the indirect activation model for BAX and BAK. However, dynamic interactions occur between BAX and activator BH3s, including tBID, BIM, and PUMA (*18*), which helps explain the previous difficulty in detecting these interactions. Here, we demonstrate an essential role of BID, BIM, and PUMA in activating BAX and BAK and for some apoptotic events during development. Our genetic study indicates that BAD is unable to induce apoptosis in the absence of BID, BIM, and PUMA, which is further supported by the observation that the BAD mimetic, ABT-737 (*29*), failed to kill *Bid*$^{-/-}$*Bim*$^{-/-}$*Puma*$^{-/-}$ TKO cells (fig. S15). These data suggest that the profound block of apoptosis conferred by the triple deficiency of *Bid*, *Bim*, and *Puma* is not simply caused by altering the ratio between antiapoptotic and proapoptotic BCl-2 proteins. BH3s not only induce BAX- and BAK-dependent release of cytochrome c to activate caspases but also initiate caspase-independent mitochondrial dysfunction (*9*). Accordingly, persistent interdigital webs and accumulation of hematopoietic cells were observed in *Bax*$^{-/-}$*Bak*$^{-/-}$ DKO (*21*) or *Bid*$^{-/-}$*Bim*$^{-/-}$*Puma*$^{-/-}$ TKO mice, but not in *Apaf-1*–deficient mice (*28*, *30*). Overall, our study reveals an essential axis of activator BH3s and BAX and BAK in activating the mitochondrial death program, which offers common ground for therapeutic interventions.

References and Notes

1. A. Gross, J. M. McDonnell, S. J. Korsmeyer, *Genes Dev.* **13**, 1899 (1999).
2. X. Wang, *Genes Dev.* **15**, 2922 (2001).
3. D. D. Newmeyer, S. Ferguson-Miller, *Cell* **112**, 481 (2003).
4. J. C. Reed, *Cell Death Differ.* **13**, 1378 (2006).
5. R. J. Youle, A. Strasser, *Nat. Rev. Mol. Cell Biol.* **9**, 47 (2008).
6. S. Desagher *et al.*, *J. Cell Biol.* **144**, 891 (1999).
7. M. C. Wei *et al.*, *Genes Dev.* **14**, 2060 (2000).
8. M. C. Wei *et al.*, *Science* **292**, 727 (2001).
9. E. H. Cheng *et al.*, *Mol. Cell* **8**, 705 (2001).
10. A. Letai *et al.*, *Cancer Cell* **2**, 183 (2002).
11. T. Kuwana *et al.*, *Mol. Cell* **17**, 525 (2005).
12. H. Kim *et al.*, *Nat. Cell Biol.* **8**, 1348 (2006).
13. H. L. Galonek, J. M. Hardwick, *Nat. Cell Biol.* **8**, 1317 (2006).
14. T. Kuwana *et al.*, *Cell* **111**, 331 (2002).
15. J. F. Lovell *et al.*, *Cell* **135**, 1074 (2008).
16. E. Gavathiotis *et al.*, *Nature* **455**, 1076 (2008).
17. S. N. Willis *et al.*, *Science* **315**, 856 (2007).
18. H. Kim *et al.*, *Mol. Cell* **36**, 487 (2009).
19. M. Certo *et al.*, *Cancer Cell* **9**, 351 (2006).
20. N. Y. Fu, S. K. Sukumaran, S. Y. Kerk, V. C. Yu, *Mol. Cell* **33**, 15 (2009).
21. T. Lindsten *et al.*, *Mol. Cell* **6**, 1389 (2000).
22. F. Tronche *et al.*, *Nat. Genet.* **23**, 99 (1999).
23. T. M. Miller *et al.*, *J. Cell Biol.* **139**, 205 (1997).
24. G. V. Putcha *et al.*, *J. Cell Biol.* **157**, 441 (2002).
25. C. G. Besirli, E. F. Wagner, E. M. Johnson Jr., *J. Cell Biol.* **170**, 401 (2005).
26. C. A. Harris, E. M. Johnson Jr., *J. Biol. Chem.* **276**, 37754 (2001).
27. J. E. Chipuk *et al.*, *Proc. Natl. Acad. Sci. U.S.A.* **105**, 20327 (2008).
28. V. S. Marsden *et al.*, *Nature* **419**, 634 (2002).
29. T. Oltersdorf *et al.*, *Nature* **435**, 677 (2005).
30. H. Yoshida *et al.*, *Cell* **94**, 739 (1998).

31. We apologize to all the investigators whose research could not be appropriately cited owing to space limitation. We thank T. D. Westergard and H.-F. Chen for technical assistance. This work was supported by grants to E.H.-Y.C. from NIH (R01CA125562) and the Searle Scholars Program, and to G.P.Z. from NIH (R01GM083159 and P30CA21765)

Supporting Online Material

www.sciencemag.org/cgi/content/full/330/6009/1390/DC1
Materials and Methods
Figs. S1 to S15
Tables S1 and S2
References

30 March 2010; accepted 14 October 2010
10.1126/science.1190217

Arabidopsis Type I Metacaspases Control Cell Death

Nuria S. Coll,[1] Dominique Vercammen,[2]* Andrea Smidler,[1] Charles Clover,[1]† Frank Van Breusegem,[2] Jeffery L. Dangl,[1,3,4]‡ Petra Epple[1]‡

Metacaspases are distant relatives of animal caspases found in protozoa, fungi, and plants. Limited experimental data exist defining their function(s), despite their discovery by homology modeling a decade ago. We demonstrated that two type I metacaspases, AtMC1 and AtMC2, antagonistically control programmed cell death in *Arabidopsis*. AtMC1 is a positive regulator of cell death and requires conserved caspase-like putative catalytic residues for its function. AtMC2 negatively regulates cell death. This function is independent of the putative catalytic residues. Manipulation of the *Arabidopsis* type I metacaspase regulatory module can nearly eliminate the hypersensitive cell death response (HR) activated by plant intracellular immune receptors. This does not lead to enhanced pathogen proliferation, decoupling HR from restriction of pathogen growth.

Programmed cell death is essential for plant development (*1*). Metacaspases in plants, fungi, and protozoa are distant homologs of caspases in the CD cysteine protease superfamily (caspases, paracaspases, gingipains, clostripains, legumains, and separin). These evolutionarily related proteases share the caspase-hemoglobinase fold, and common catalytic-site domains (*2*, *3*). The *Arabidopsis thaliana* genome encodes three type I and six type II metacaspases (AtMCs) (*3*). Both types contain a conserved putative catalytic domain and plausible sites for autocatalytic processing but differ in their N-terminal domains. Despite many reports of caspase-like activities in plants (*4*–*9*), no experimental data exist defining functions or substrates for plant type I metacaspases. Type II metacaspase functions are nearly as enigmatic: Recombinant plant type II metacaspases AtMC4 and AtMC9 can undergo in vitro autocatalytic processing (*10*), and the Tudor staphylococcal nuclease, cleaved during programmed cell death in pine, is the only in vivo type II metacaspase substrate defined in plants (*11*). Although classic animal caspases cleave after an aspartate at the P1 position, metacaspases cleave after a basic amino acid residue such as lysine or arginine (*9*).

LSD1 is a negative regulator of cell death initiated by localized superoxide production occurring during the hypersensitive response (HR), a cell death that often accompanies pathogen recognition. HR sites form normally in *lsd1* (*12*), but the typical sharp boundary between dead and live cells subsequently breaks down and "runaway cell death" ensues throughout the leaf (*12*). This phenotype requires proteins that are also necessary for pathogen recognition and salicylic acid accumulation (*12*–*16*). Hence, *lsd1* is a sensitized genetic background for studying the control of oxidative stress–dependent cell death (*17*–*20*).

All three type I *Arabidopsis* metacaspases, *AtMC1* (At1g02170), *AtMC2* (At4g25110), and *AtMC3* (At5g64240), possess a conserved, plant-specific *LSD1*-like zinc-finger N-terminal motif (CxxCRxxLMYxxGASxVxCxxC) (*21*) (fig. S1A). The LSD1 zinc-finger domain can function in protein interactions (*22*). In yeast, LSD1 and AtMC1 interact via their zinc-finger domains (fig. S1, B to D). In contrast, AtMC2 interacts only very weakly with either AtMC1 or LSD1 in this assay (fig. S1, B to D). We substantiated the AtMC1-LSD1 interaction using in vivo coimmunoprecipitation in transgenic *Arabidopsis* (Fig. 1B) and in transient expression assays in *Nicotiana benthamiana* (*23*) (fig. S2A). The predicted N-terminal prodomain of AtMC1 is required for interaction with

[1]Department of Biology, 108 Coker Hall, University of North Carolina (UNC), CB 3280, Chapel Hill, NC 27599–3280, USA. [2]VIB Department of Plant Systems Biology and Department of Plant Biotechnology and Genetics, Ghent University, 9052 Ghent, Belgium. [3]Curriculum in Genetics and Molecular Biology and Department of Microbiology and Immunology, UNC, Chapel Hill, NC 27599, USA. [4]Carolina Center for Genome Sciences, UNC, Chapel Hill, NC 27599, USA.

*Present address: Innogenetics, Technologiepark 6, 9052 Ghent, Belgium.

†Present address: Department of Anesthesiology, Wake Forest University School of Medicine, Medical Center Boulevard, Winston-Salem, NC 27157, USA.

‡To whom correspondence should be addressed. E-mail: pepple@email.unc.edu (P.E.); dangl@email.unc.edu (J.L.D.)

LSD1 (fig. S2A). AtMC2 does not coimmunoprecipitate with either LSD1 (fig. S2B) or AtMC1 (fig. S2C) under these conditions.

We obtained transfer DNA (T-DNA) insertional mutant alleles of *atmc1*, *atmc2*, and *lsd1* in the Col-0 accession (Fig. 1A and fig. S1B). *atmc1*, *atmc2*, and the *atmc1 atmc2* double mutant exhibited no signs of enhanced production of reactive oxygen species and had no obvious phenotypes (fig. S3). We generated *lsd1 atmc1* and *lsd1 atmc2* double mutants, and the *lsd1 atmc1 atmc2* triple mutant to determine whether *atmc1* or *atmc2* modifies the *lsd1* cell death phenotype. *lsd1* runaway cell death can be induced with benzo(1,2,3)thiadiazole-7-carbothioic acid *S*-methyl ester (BTH), a salicylic acid analog (*16*). *lsd1* exhibited maximum ion leakage (a cell death proxy) 96 hours after BTH treatment. The Col-0 wild type, *atmc1*, *atmc2*, and *atmc1 atmc2* did not display significant increases in ion leakage (Fig. 2A). *lsd1 atmc1* exhibited suppressed BTH-induced ion leakage (Fig. 2A, left). In contrast, *lsd1 atmc2* displayed accelerated BTH-induced ion leakage (Fig. 2A, right). Ion leakage in *lsd1 atmc1 atmc2* was similar to that in *lsd1 atmc1* (Fig. 2A, right). Consistent with these data, morphological *lsd1* phenotypes were abolished in the absence of *AtMC1*, and more pronounced in the *lsd1 atmc2* mutant (fig. S3). Hence, AtMC1 is a positive mediator of *lsd1* runaway cell death, and AtMC2 acts genetically as a negative regulator of AtMC1.

Hemagglutinin (HA)–epitope-tagged *AtMC1* and *AtMC2* constructs controlled by their native promoters (*pAtMC1::AtMC1-HA* and *pAtMC2::AtMC2-HA*) complemented the respective mutant phenotypes for BTH-induced ion leakage in *lsd1* (Fig. 2B). AtMC1-HA protein was detectable 1 day after BTH spray, before plants displayed any visible sign of cell death, and accumulated thereafter (Fig. 2C). AtMC2-HA was undetectable until 2 days after BTH treatment and accumulated to lower levels than AtMC1-HA (Fig. 2C). We observed no HA-tagged low-molecular-weight products, suggesting either a lack of processing during activation or instability of a putative C-terminal HA-tagged fragment.

We monitored *AtMC1* or *AtMC2* expression in transgenic plants carrying promoter β-glucuronidase (*GUS*) reporter genes (*pAtMC1::GUS* and *pAtMC2::GUS*, respectively) in either Col-0 or *lsd1*. *AtMC1* expression was confined to the leaf veins. However, 24 hours after BTH treatment, *AtMC1* was expressed in a narrow zone of several cells adjacent to cell death sites in *lsd1* (fig. S4A). Cells expressing *AtMC1* are destined to die as runaway cell death expands over time (*15*). *AtMC2*, in contrast, was expressed at low levels, except for a halo of nonstained cells outlining cells that are committed to die (fig. S4B).

We infected Col-0 *pAtMC1::GUS* and *pAtMC2::GUS* transgenic plants with either the obligate biotrophic oomycete *Hyaloperonospora arabidopsidis* (*Hpa*; isolate Emwa1), or the hemibiotrophic bacte-

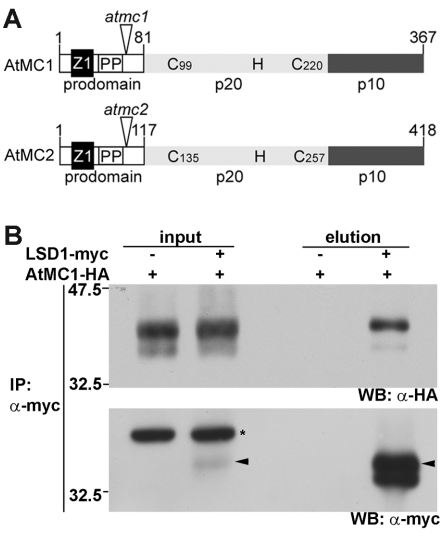

Fig. 1. AtMC1 interacts with LSD1. (**A**) Scheme of AtMC1 and AtMC2 proteins (not to scale). Z1, LSD1-like zinc finger; PP, proline-rich region; p20 and p10, putative caspase-like catalytic domains (*2*); numbered H and C, putative catalytic residues (*2*); *atmc1* and *atmc2*, T-DNA insertion sites. (**B**) AtMC1 and LSD1 coimmunoprecipitate. Protein extracts from leaves of *lsd1 atmc1* [*pLSD1::LSD1-myc*] × *lsd1 atmc1* [*Dex-AtMC1-HA*] F_1 plants were immunoprecipitated with anti-myc–coupled magnetic beads. Crude extract (input) and eluate (elution) were analyzed by SDS–polyacrylamide gel electrophoresis (SDS-PAGE) with anti-HA (top) or anti-myc (bottom) immunoblot. The eluate is 8× concentrated as compared to the input. The asterisk denotes a nonspecific cross-reacting band; arrowheads are ~34 kD, the expected apparent molecular mass of LSD1-myc. WB, Western blot.

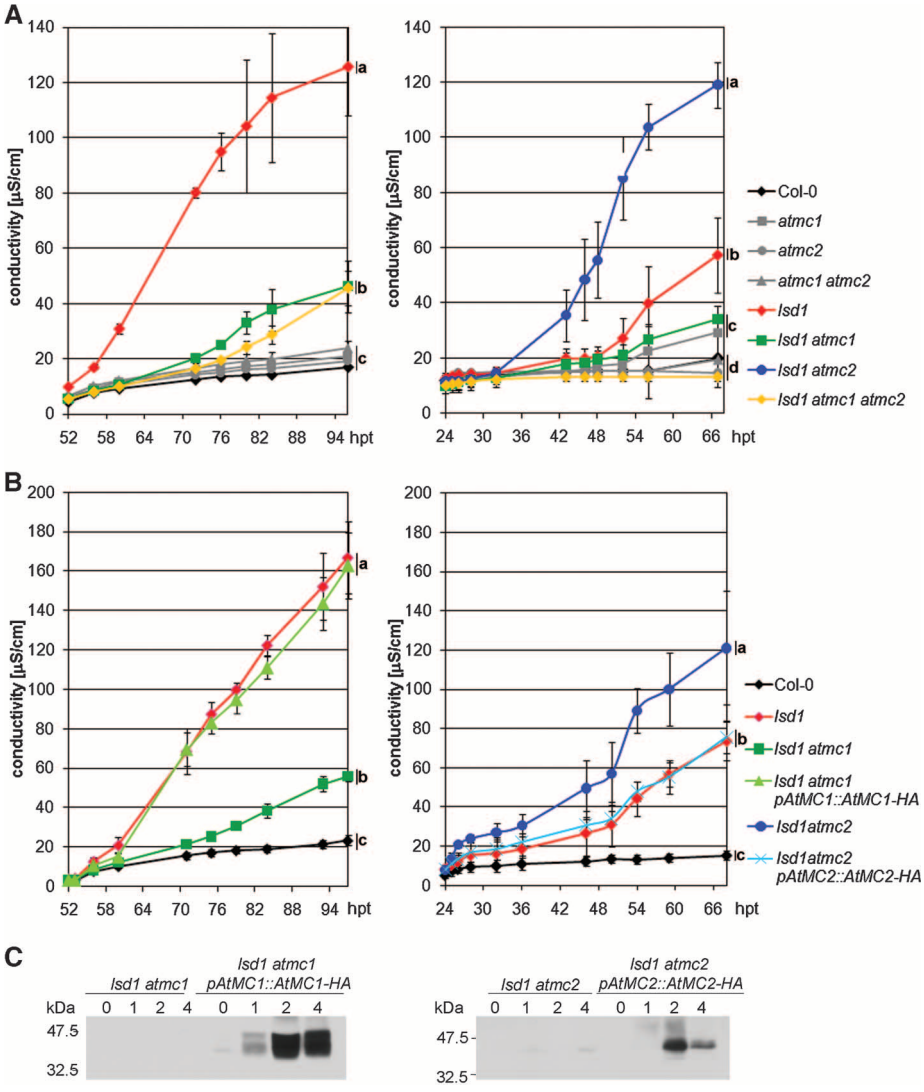

Fig. 2. *AtMC1* and *AtMC2* antagonistically control *lsd1* runaway cell death. (**A** and **B**) Four-week-old homozygous transgenic plants (genotypes, right) were sprayed with 150 μM BTH, and conductivity was measured at the time points indicated. Repeated three times in (A) and once in (B). Error bars indicate two times the standard error, calculated from four replicate measurements per genotype and data point. Letters a to d at right represent groups with significant differences [$P < 0.05$, Tukey's honest significant difference (HSD) test]. hpt, hours post treatment. (**C**) Four-week-old plants of the indicated genotypes were sprayed with 150 μM BTH. Tissue was harvested at the indicated time points, and 50 μg of total protein were analyzed by SDS-PAGE and anti-HA immunoblot.

ria *Pseudomonas syringae* pv. *tomato* [*Pto*; strain DC3000(*avrRpm1*)] to trigger HR via the specific intracellular Toll–interleukin-1 receptor (TIR) and coiled-coil (CC)–nucleotide-binding–leucine-rich repeat (NB-LRR) immune receptors RPP4 (*24*) and RPM1 (*25*), respectively. *AtMC1* was activated upon NB-LRR–based pathogen recognition and subsequently expressed in a spatially restricted manner in cells destined to undergo HR (fig. S5). In contrast, *AtMC2* was expressed in a relatively more diffuse zone around infection sites (fig. S5).

We generated transgenic plants conditionally expressing either a full-length or an N-terminal truncated version of *AtMC1* lacking the *LSD1*-like extension (*AtMC1-HA* and *AtMC1-ΔN-HA,* respectively). High levels of AtMC1-HA accumulation resulted in cell death in Col-0 transgenics; lower levels did not (Fig. 3A). Col-0 *AtMC1-ΔN-HA* plants accumulating relatively low levels of protein nevertheless exhibited enhanced cell death (Fig. 3A). We failed to recover transgenics expressing *AtMC1-ΔN-HA* in *lsd1* either by direct transformation or from crosses of two independent Col-0 *AtMC1-ΔN-HA*-expressing transgenic lines to *lsd1* [see methods in supporting online material (SOM)]. These results suggest that the *LSD1*-like putative prodomain of AtMC1 negatively regulates its pro–cell death activity.

Typical caspase active sites include a histidine-cysteine catalytic dyad, also found in metacaspases (*3*). The predicted catalytic cysteine residue was essential for autoprocessing of the pine metacaspase mcII-Pa (*26*), of *Arabidopsis* AtMC4 and AtMC9 in bacteria (*10*), and of AtMC1 and AtMC5 in yeast (*27*). In *Trypanosoma brucei* metacaspase *TbMCA4*, a second, metacaspase-specific cysteine residue was catalytic, and the corresponding residue compensated for mutation of the classic cysteine residue in AtMC9 (*28*, *29*). We generated Col-0 transgenic lines expressing high or low levels of either a conditional AtMC1 expression construct containing a cysteine-to-alanine mutation (*AtMC1-C220A-HA*) or a double mutation including the potentially compensatory cysteine (*AtMC1-C99A-C220A-HA*) (Fig. 3B). Conditional overexpression of *AtMC1-HA* resulted in a dose-dependent increase in ion leakage, whereas overexpression of either *AtMC1-C220A-HA* or *AtMC1-C99A-C220A-HA* did not (Fig. 3C). Hence, AtMC1-C220 is required for function, and AtMC1-C99 cannot compensate for its loss.

Overexpression of *AtMC1* did not induce cell death in cotyledons before infection. However, massive cell death occurred after infection with *Hpa* and activation of RPP4 (Fig. 3, D and E). Hence, AtMC1 activation in seedlings, in contrast to adult plants (Fig. 3A), requires an additional signal, which is consistent with the fact that *lsd1* runaway cell death also does not occur in cotyledons.

We generated similar transgenics in *lsd1* and Col-0 that conditionally expressed full-length *AtMC2* (*AtMC2-HA*), an analogous N-terminal truncated version of *AtMC2* (*AtMC2-ΔN-HA*) and either *AtMC2* or *AtMC2-ΔN* with cysteine-to-alanine mutations in the predicted catalytic (C256) and potentially compensatory (C135) cysteine residues (*AtMC2-C135A-C256A-HA* and *AtMC2-ΔN-C135A-C256A-HA*). BTH-induced *lsd1* runaway cell death was suppressed in transgenic lines expressing full-length *AtMC2-HA* (fig. S6, A and B). Cell death suppression was nearly complete in *AtMC2-ΔN-HA*–expressing lines (Fig. 4A and figs. S6C and S7). Surprisingly, the predicted catalytic cysteines were not required for cell death suppression by either AtMC2 or AtMC2-ΔN-HA (Fig. 4A and fig. S6B).

To assess whether AtMC2 suppressed NB-LRR–mediated HR, we infected Col-0, *atmc1*, *atmc2*, *atmc1 atmc2*, and transgenic plants expressing *AtMC2-ΔN-HA* or *AtMC2-ΔN-C135A-C256A-HA* with *Pto* DC3000(*avrRpm1*). We observed enhancement of RPM1-mediated HR in *atmc2* (Fig. 4B). Conversely, we observed suppression of RPM1-mediated HR in *atmc1* and in *atmc1 atmc2* at low bacterial inocula resembling natural infections (Fig. 4B), but not at artificially high doses. Conditional expression of either *AtMC2-ΔN* (Fig. 4C and fig. S6F) or full-length *AtMC2* (fig. S6, D and E) suppressed RPM1-mediated HR, phenocopying *atmc1*.The suppression of HR did not result in increased susceptibility to *Pto* DC3000(*avrRpm1*) (Fig. 4, D and E). RPP4-mediated HR was also suppressed by conditional expression of *AtMC2-ΔN* and in *atmc1* (Fig. 4F). Thus, AtMC2 inhibits at least RPM1- and RPP4- mediated HR, via direct or indirect regulation of AtMC1. The putative catalytic sites of AtMC2 are not required for HR suppression (Fig. 4, B, C, and F, and fig. S6E). *atmc2* did not exhibit increased RPP4-mediated HR (*30*). Although *Hpa* Emwa1 is an obligate biotrophic oomycete, AtMC2-ΔN–mediated suppression of HR did not abolish RPP4-dependent pathogen growth restriction (Fig. 4F). These surprising observations are consistent with pre-

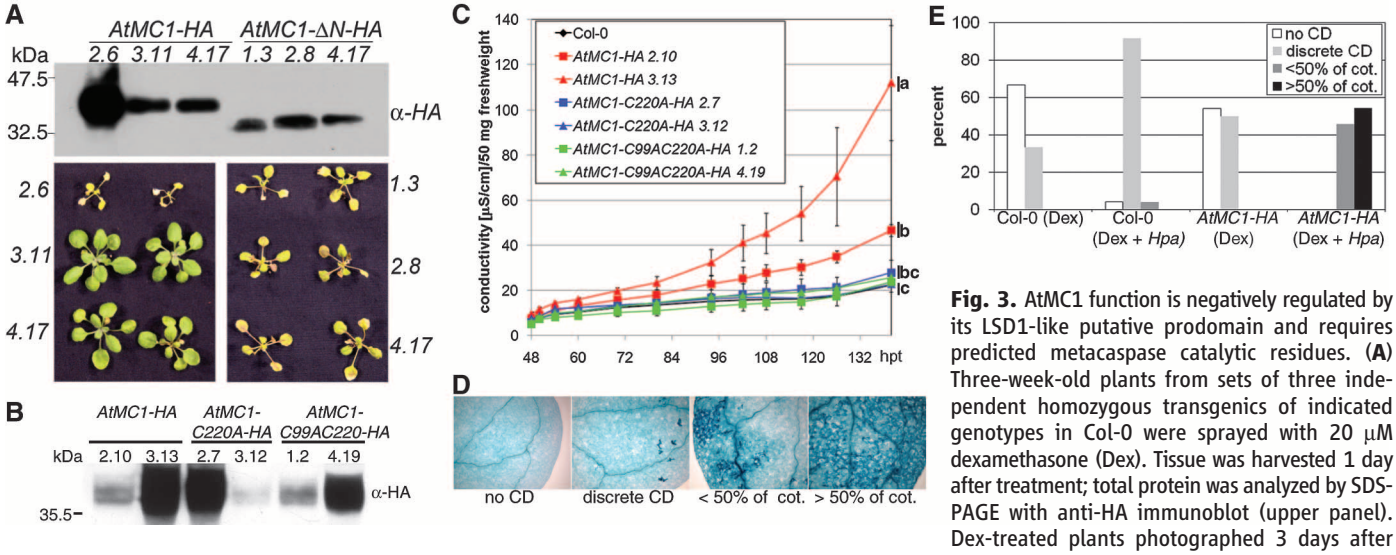

Fig. 3. AtMC1 function is negatively regulated by its LSD1-like putative prodomain and requires predicted metacaspase catalytic residues. (**A**) Three-week-old plants from sets of three independent homozygous transgenics of indicated genotypes in Col-0 were sprayed with 20 μM dexamethasone (Dex). Tissue was harvested 1 day after treatment; total protein was analyzed by SDS-PAGE with anti-HA immunoblot (upper panel). Dex-treated plants photographed 3 days after treatment are shown (lower panel). (**B**) As in (A), but using two independent transgenics of the genotypes listed above the blot. (**C**) AtMC1-mediated ion leakage requires the putative catalytic cysteine residue C220. Plants treated as described in (A) were harvested at 46 hpt and processed as described in the SOM. Error bars represent two times the standard error. Letters a to c represent experimental groups with significant differences ($P < 0.05$, Tukey's HSD test). The experiment was repeated twice. (**D** and **E**) *AtMC1* function in cotyledons requires additional signals. Ten-day-old seedlings were pre-treated with 20 μM Dex (+Dex). One day later, half of the seedlings were inoculated with 50,000 spores/ml of *Hpa* isolate Emwa1 (Dex + *Hpa*) to activate RPP4. All seedlings were harvested 3 days after inoculation and stained with Trypan blue to visualize cell death. (D) Pictures of representative Trypan blue–stained cotyledons. (E) 20 cotyledons were evaluated per genotype and treatment. CD, cell death; <50% of cot., extensive cell death covering less than 50% of cotyledon; >50% of cot., extensive cell death covering more than 50% of cotyledon.

vious results showing that HR can occur in the absence of pathogen growth restriction and that HR can be inhibited by caspase inhibitors (*6*, *31*). The pathogen-stress marker PR1 is not induced by *AtMC2-ΔN* overexpression, suggesting that these results are not a general consequence of stress. Finally, AtMC2 control of AtMC1 is post-transcriptional (fig. S7).

Our data establish AtMC1 as a pro-death caspase-like protein required for both superoxide-dependent cell death in a reactive oxygen–sensitized state and for full HR mediated by intracellular NB-LRR immune receptor proteins. AtMC2 antagonizes these functions. AtMC1 and AtMC2 contain a plant-specific N terminus shared with LSD1. The functions of both AtMC1 and AtMC2 are enhanced by removal of this domain and, at least for AtMC1, this domain is required for interaction with LSD1. In the absence of LSD1, AtMC1-dependent cell death requires additional, unknown signals and is developmentally regulated. Hence, activation of AtMC1 is complex and probably context-dependent. The inhibitory function of AtMC2 does not require classic cysteine catalytic residues. The AtMC1-AtMC2 antagonism is reminiscent of animal caspase-12, which negatively regulates caspase-1 to dampen the inflammatory response to bacteria and in colitis-associated colorectal cancer (*32*, *33*); these caspase-12 functions do not require catalytic function (*33*). Caspase-12 also inhibits NOD-like receptor-mediated innate immunity independent of caspase-1 (*34*), providing a striking parallel to our observation that AtMC2 inhibits AtMC1-dependent cell death controlled by analogous plant NB-LRR innate immune receptors. These results suggest an ancient link between cell death control by divergent metacaspase/caspase proteases and innate immune receptor function governed by NB-LRR or NLR proteins.

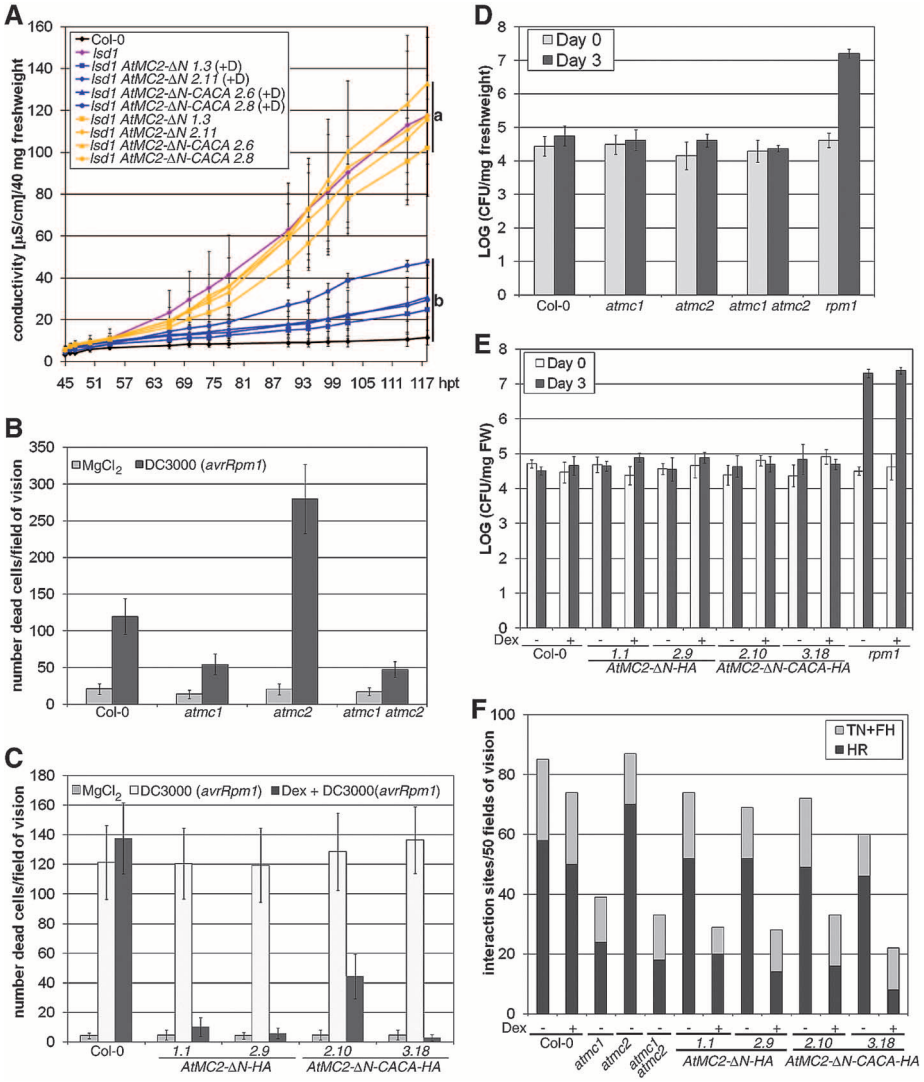

Fig. 4. AtMC2 negatively regulates AtMC1. Seedlings of the depicted genotypes were sprayed with 1 µM Dex 6, 11, and 16 days after germination or left unsprayed. CACA denotes constructs where both putative catalytically active cysteine residues (C135A C256A for AtMC2) were mutated to alanine. (**A**) For ion leakage measurements, plants were sprayed with 150 µM BTH 1 day after the last treatment with Dex. Tissue was harvested at 43 hpt and processed as described in the SOM. Blue lines, Dex-treated genotypes; yellow lines, non–Dex-treated controls. Error bars represent two times the standard error. Letters a and b at right represent experimental groups with significant differences ($P < 0.05$, Tukey's HSD test). The experiment was repeated twice. (**B**) Plants were vacuum-infiltrated with 250,000 colony-forming units (CFU)/ml of *Pto* DC3000(*avrRpm1*). Twelve hours later, plants were harvested and stained with Trypan blue to visualize cell death. To quantify cell death, all dead cells in one field of vision (10× magnification) were counted. Average and two times the standard error were calculated from 20 leaves per genotype and treatment. The experiment was repeated. (**C**) Ten hours after the last treatment with Dex, plants of indicated genotypes were treated as in (B). (**D**) Seedlings were dip-infiltrated with *Pto* DC3000(*avrRpm1*) at 2.5×10^7 CFU/ml. The average and two times the standard error were calculated from four samples per genotype. The experiment is representative of three independent replicates. (**E**) Three hours after the last Dex spray, plants were treated as in (D). (**F**) One day after the last Dex treatment, plants were inoculated with 50,000 spores/ml of *Hpa* Emwa1. Three days later, plants were stained with Trypan blue, and interaction sites per field of vision were counted. The experiment was repeated three times. TN, trailing necrosis; FH, free hyphae.

References and Notes

1. E. Lam, *Nat. Rev. Mol. Cell Biol.* **5**, 305 (2004).
2. L. Aravind, E. V. Koonin, *Proteins* **46**, 355 (2002).
3. A. G. Uren *et al.*, *Mol. Cell* **6**, 961 (2000).
4. N. V. Chichkova *et al.*, *EMBO J.* **29**, 1149 (2010).
5. N. Hatsugai *et al.*, *Genes Dev.* **23**, 2496 (2009).
6. N. Hatsugai *et al.*, *Science* **305**, 855 (2004).
7. E. Lam, O. del Pozo, *Plant Mol. Biol.* **44**, 417 (2000).
8. E. Rojo *et al.*, *Curr. Biol.* **14**, 1897 (2004).
9. D. Vercammen, W. Declercq, P. Vandenabeele, F. Van Breusegem, *J. Cell Biol.* **179**, 375 (2007).
10. D. Vercammen *et al.*, *J. Biol. Chem.* **279**, 45329 (2004).
11. J. F. Sundström *et al.*, *Nat. Cell Biol.* **11**, 1347 (2009).
12. R. A. Dietrich *et al.*, *Cell* **77**, 565 (1994).
13. R. A. Dietrich, M. H. Richberg, R. Schmidt, C. Dean, J. L. Dangl, *Cell* **88**, 685 (1997).
14. D. H. Aviv *et al.*, *Plant J.* **29**, 381 (2002).
15. T. Jabs, R. A. Dietrich, J. L. Dangl, *Science* **273**, 1853 (1996).
16. C. Rustérucci, D. H. Aviv, B. F. Holt 3rd, J. L. Dangl, J. E. Parker, *Plant Cell* **13**, 2211 (2001).
17. A. Mateo *et al.*, *Plant Physiol.* **136**, 2818 (2004).
18. P. Mühlenbock, M. Plaszczyca, M. Plaszczyca, E. Mellerowicz, S. Karpinski, *Plant Cell* **19**, 3819 (2007).
19. P. Mühlenbock *et al.*, *Plant Cell* **20**, 2339 (2008).
20. M. A. Torres, J. D. Jones, J. L. Dangl, *Nat. Genet.* **37**, 1130 (2005).
21. Single-letter abbreviations for the amino acid residues are as follows: A, Ala; C, Cys; D, Asp; E, Glu; F, Phe; G, Gly; H, His; I, Ile; K, Lys; L, Leu; M, Met; N, Asn; P, Pro; Q, Gln; R, Arg; S, Ser; T, Thr; V, Val; W, Trp; Y, Tyr; and x, any amino acid.
22. H. Kaminaka *et al.*, *EMBO J.* **25**, 4400 (2006).
23. Materials and methods are available as supporting material on *Science* Online.
24. E. A. van der Biezen, C. T. Freddie, K. Kahn, J. E. Parker, J. D. Jones, *Plant J.* **29**, 439 (2002).
25. M. R. Grant *et al.*, *Science* **269**, 843 (1995).
26. P. V. Bozhkov *et al.*, *Proc. Natl. Acad. Sci. U.S.A.* **102**, 14463 (2005).
27. N. Watanabe, E. Lam, *J. Biol. Chem.* **280**, 14691 (2005).
28. B. Belenghi *et al.*, *J. Biol. Chem.* **282**, 1352 (2007).
29. A. Szallies, B. K. Kubata, M. Duszenko, *FEBS Lett.* **517**, 144 (2002).
30. Because this assay counts interaction sites, the number of spores that infect each leaf determines the maximum number of interactions that can occur per leaf. This cannot be altered by an increase in RPP4-dependent responses.

31. K. S. Century, E. B. Holub, B. J. Staskawicz, *Proc. Natl. Acad. Sci. U.S.A.* **92**, 6597 (1995).
32. J. Dupaul-Chicoine *et al.*, *Immunity* **32**, 367 (2010).
33. M. Saleh *et al.*, *Nature* **440**, 1064 (2006).
34. P. M. LeBlanc *et al.*, *Cell Host Microbe* **3**, 146 (2008).
35. We thank J. McDowell (Virginia Tech, Blacksburg, VA) and M. Nishimura (UNC) for critical reading of the manuscript. This work was funded by NIH RO1 GM057171 to J.L.D.; a Swiss National Science Foundation Fellowship (PBEZA-115173) to N.S.C.; and the Research Fund, Ghent University (grant 12051403), and Fonds voor Wetenschappelijk Onderzoek-Vlaanderen to F.V.B. and D.V., respectively. We thank D. Baltrus for statistical analysis, T. Perdue of the UNC Biology Microscope Facility for patient and expert assistance, E. Washington and T. Eitas for pMDC7 vectors, B. van de Cotte for technical assistance, and K. Overmyer for early contributions to this work.

Supporting Online Material
www.sciencemag.org/cgi/content/full/science.1194980/DC1
Materials and Methods
Figs. S1 to S7
References

12 July 2010; accepted 19 October 2010
Published online 18 November 2010;
10.1126/science.1194980

An Antagonistic Pair of *FT* Homologs Mediates the Control of Flowering Time in Sugar Beet

Pierre A. Pin,[1,2] Reyes Benlloch,[1] Dominique Bonnet,[3] Elisabeth Wremerth-Weich,[2] Thomas Kraft,[2] Jan J. L. Gielen,[3] Ove Nilsson[1]*

Cultivated beets (*Beta vulgaris* ssp. *vulgaris*) are unable to form reproductive shoots during the first year of their life cycle. Flowering only occurs if plants get vernalized, that is, pass through the winter, and are subsequently exposed to an increasing day length (photoperiod) in spring. Here, we show that the regulation of flowering time in beets is controlled by the interplay of two paralogs of the *FLOWERING LOCUS T (FT)* gene in *Arabidopsis* that have evolved antagonistic functions. *BvFT2* is functionally conserved with *FT* and essential for flowering. In contrast, *BvFT1* represses flowering and its down-regulation is crucial for the vernalization response in beets. These data suggest that the beet has evolved a different strategy relative to *Arabidopsis* and cereals to regulate vernalization.

In flowering plants, the timing of the transition from the vegetative to the reproductive stage is determined by interactions between the developmental state of the plant and exogenous stimuli, such as changes in day length and temperature. Vernalization is a checkpoint through which many plants must pass, where flowering is conditional on prolonged exposure to cold temperature and is subsequently induced by other inductive pathways (*1*). Vernalization of the winter-annual *Arabidopsis* and other members of the *Brassicaceae* family involve several steps that culminate in the repression of the major floral inhibitor gene *FLOWERING LOCUS C* (*FLC*) (*2*–*5*). In cereals, cold temperature stimuli are integrated by the activation of the *FRUITFULL* (*FUL*)/*APETALA1* (*AP1*) homolog *VRN1* (*6*), which represses the CONSTANS, CONSTANS-like, and TIMING OF CAB EXPRESSION 1 (CCT)-domain transcription factor *VRN2* (*7*, *8*).

The phosphatidylethanolamine-binding protein (PEBP) gene family, found in both angiosperms and gymnosperms (*9*), has evolved both activators and repressors of flowering. The *Arabidopsis*

[1]Umeå Plant Science Centre, Department of Forest Genetics and Plant Physiology, Swedish University of Agricultural Sciences, 901-83 Umeå, Sweden. [2]Syngenta Seeds AB, Box 302, 261-23 Landskrona, Sweden. [3]Syngenta Seeds SAS, 12 Chemin de l'Hôbit, 31790 Saint-Sauveur, France.

*To whom correspondence should be addressed. E-mail: Ove.Nilsson@genfys.slu.se

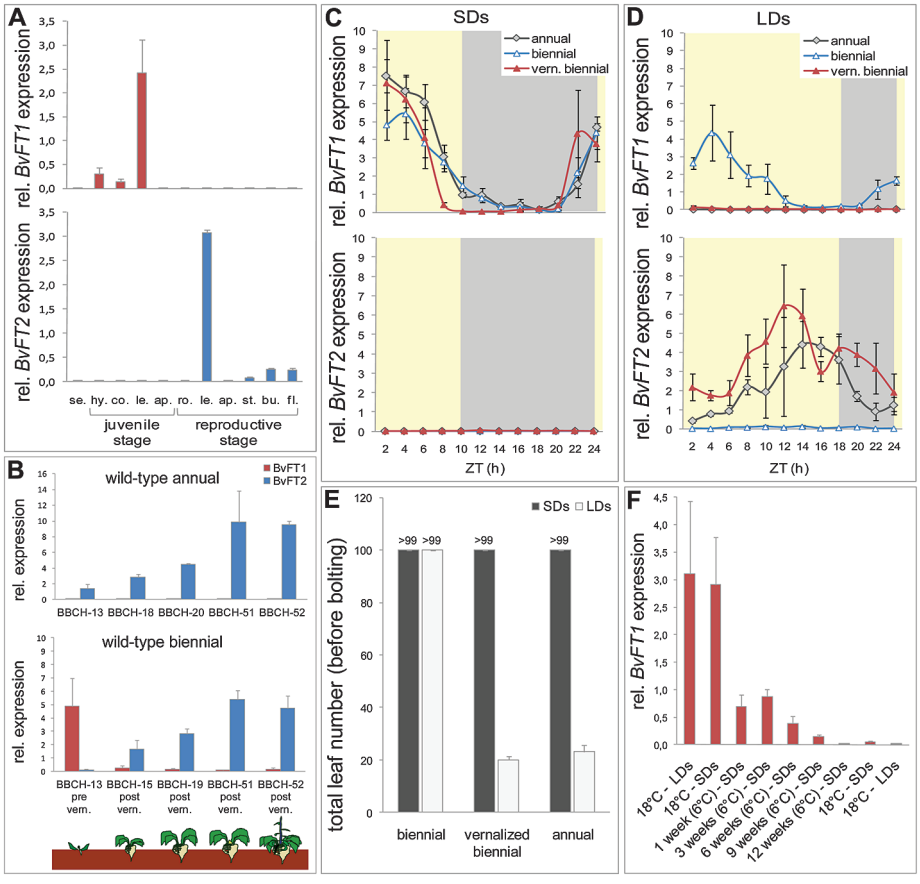

Fig. 1. Expression pattern of *BvFT1* and *BvFT2* in beets (*15*). (**A**) Expression of *BvFT1* and *BvFT2* in various tissues, including se., seed; hy., hypocotyl; co., cotyledon; le., leaf; ap., apex; ro., root; st., stem; bu., floral bud, and fl., flower. Samples were harvested in LDs at zeitgeber time (ZT) 8 (i.e., 8 hours after lights on). Error bars, mean ± SE (n = 3). (**B**) Expression of *BvFT1* and *BvFT2* in leaf samples in LDs across different developmental stages in annuals and biennials. Samples were harvested at ZT6. Error bars, mean ± SE (n = 3). (**C** and **D**) Diurnal rhythms of *BvFT1* and *BvFT2* in annual, biennial, and vernalized-biennial beets in SDs (C) and LDs (D). Error bars, mean ± SE (n = 5). (**E**) Leaf number at time of bolting in biennial, vernalized-biennial, and annual plants grown under the different photoperiodic conditions described in (C) and (D). Error bars, mean ± SD (n = 6). (**F**) *BvFT1* transcript accumulation in biennials in response to vernalization. Leaf samples were harvested at ZT6. Error bars, mean ± SE (n = 3).

Supporting Online Material for

Arabidopsis Type I Metacaspases Control Cell Death

Nuria S. Coll, Dominique Vercammen, Andrea Smidler, Charles Clover, Frank van Breusegem, Jeffery L. Dangl,* Petra Epple*

*To whom correspondence should be addressed. E-mail: pepple@email.unc.edu (P.E.); dangl@email.unc.edu (J.L.D.)

Published 18 November 2010 on *Science* Express
DOI: 10.1126/science.1194980

This PDF file includes:

MATERIALS AND METHODS

Plant Materials and Growth Conditions

We used *Arabidopsis thaliana* Columbia (Col-0) and isogenic T-DNA insertional lines for *lsd1* (At4g20380; SALK_042687 (*S1*); insertion at nucleotide 57 of intron four; Arabidopsis Biological Resource Center at Ohio State University (ABRC)), *atmc1* (At1g02170, GABI_096A10; insertion at nucleotide 312 of exon one; GABI-Kat Resource, Bielefeld University, Germany) and *atmc2* (At4g25110; SALK_009045; insertion at nucleotide 255 of exon one; ABRC). All insertion sites were re-confirmed by DNA sequencing. Plants were grown under short day conditions (9 hrs light, 21°C; 15 hrs dark, 18°C).

DNA Constructs

For conditional expression of *AtMC1* and *AtMC2* and their respective mutant alleles, we cloned the appropriate full-length or truncated, C-terminally HA-epitope-tagged cDNAs into a modified version (BASTA^R) of vector pTA7002 (*S2*). A pBAR vector containing LSD1 cDNA C-terminally tagged with 6-myc and under the control of its native promoter as described in (*S3*) was used in co-immunoprecipitation experiments. For expression of *AtMC1* and *AtMC2* under control of their native promoters, HA-tagged *AtMC1* and *AtMC2* cDNAs were fused by PCR to their respective native promoters, directionally cloned into a pENTR/D/TOPO Gateway vector (Invitrogen) and recombined into the plant binary Gateway-compatible vector pGWB1 (*S4*).

For co-immunoprecipitation assays, *AtMC1* and *AtMC2* cDNAs were directionally cloned into a pENTR/D/TOPO Gateway vector (Invitrogen) and recombined into the plant binary Gateway-compatible vector pMDC7 (*S5*) with an Estradiol-inducible promoter and C-terminally-tagged with six myc epitopes (Erica Washington and Tim Eitas, personal communication).

DNA constructs were transformed by electroporation into *Agrobacterium tumefaciens* strains C58C1 (for transient transformation of *N. benthamiana* leaves) or GV3101 (for stable transformation of Arabidopsis and transient transformation of *N. benthamiana* leaves).

To inhibit post-transcriptional gene silencing in *N. benthamiana* leaves transformed with *A. tumefaciens* GV3101, the tomato bushy stunt virus silencing suppressor p19 under a 35S promoter (*S6*) was included in the infiltration mixture when pTA7002 or pBAR vectors were used.

Agrobacterium-Mediated Transformation

Arabidopsis transgenics were generated using *A. tumefaciens* (GV3101)-mediated transformation following the floral dip method as previously described (*S7*). Homozygous transgenic lines were selected on 50 µg/ml Hygromycin MS plates (pGWB1 and pMDC7) or by Basta (glufosinate-ammonium) selection (pTA7002 BASTA^R).

For *N. benthamiana* transient leaf transformation assays, *A. tumefaciens* C58C1 (pMDC7) or GV3101 (pTA7002 and pBAR) was grown overnight at 28°C on 5 ml of KB and antibiotics. Pelleted cells were resuspended in infiltration media (10 mM MES, pH 5.6, 10 mM $MgCl_2$, and

150 µM acetosyringone) and incubated at room temperature with constant rotation. After 90 minutes, cells were resuspended to the appropriate OD_{600}. Five to six-week-old *N. benthamiana* plants were inoculated by infiltration using a syringe. Infiltrated plants were kept under low light to allow transgene expression and 72 hours post-inoculation (hpi) samples were collected for further processing. Estradiol (Est) or Dexamethasone (Dex) were applied 48 h (hpi) when needed for induction of expression.

Chemical Treatments

Est or Dex (2 µM) supplemented with 0.005% Silwet were applied to *N. benthamiana* leaf surfaces using cottonballs.

For conditional induction of *AtMC1* in stable Arabidopsis transgenics, plants were sprayed once with 20 µM Dex supplemented with 0.005% Silwet. For conditional expression of *AtMC2*, 6-day-old plants were sprayed with 1 µM Dex. Subsequently, plants were sprayed every five days with 1 µM Dex until harvested for experiments.

For induction of *lsd1* runaway cell death, two- to four-week-old plants were sprayed with 150 µM benzo(1,2,3)thiadiazole-7-carbothioic acid *S*-methyl ester (BTH (0.005% Silwet)).

To monitor oxidative stress, fully expanded leaves of 4-week-old plants were infiltrated with a fresh mixture of 100 µM xanthine and 0.05 U ml^{-1} xanthine oxidase (X/XO).

Stains

Dead cells and fungal structures were visualized with Trypan Blue as described (*S8, S9*).

For Magenta-Gluc (5-bromo-6-chloro-3-indolyl-*β*-D-glucuronide; Applichem) stains, leaves were vacuum infiltrated with 1 mM Magenta-Gluc solution, and incubated over night at 37°C. Subsequently, leaves were cleared with 70% ethanol. For Magenta-Gluc/Aniline Blue double staining, ethanol-cleared, stained leaves were additionally incubated overnight in a 0.5% Aniline Blue (in 0.15 M K_2HPO_4) solution (*S10, S11*).

For Magenta-Gluc/Trypan Blue double staining, Magenta-Gluc stained leaves were incubated in boiling TB for 5 min, and then cleared with chloral hydrate.

In order to visualize accumulation of H_2O_2, leaves from 4-week-old plants grown under short-day conditions were stained with 3,3'-Diaminobenzidine (DAB) 3 days after infiltration with X/XO as previously described (*S12*).

Cell Death Assays

We tested the mutants presented in Figure 4B with concentrated inoculum (5×10^7 cfu/ml), and did not detect any differences in macroscopic HR or ion leakage. Thus, we employed lower inoculums to uncover the dose-sensitive HR phenotypes presented. We believe that this approach is justified, as it more closely resembles the low level inocula of bacterial infection occurring in nature. Our interpretation is that at extremely high doses of bacteria that we and others typically use for HR induction, several independent cell death systems are induced

subsequent to NB-LRR-mediated pathogen recognition. By lowering the dose, we not only more closely mirror natural infections, but we also resolve local infections, in the same way that use of a sporulating oomycete like *Hyaloperonospora arabidopsidis* (*Hpa*) allows analysis of single cell infections sites.

Low inoculum, single cell death assays were adapted from Hatsugai *et al.* (*S13*): leaves were vacuum infiltrated with either 250,000 cfu/ml (Fig 4B) or 500,000 cfu/ml (Fig. 4C and fig. S6E) *Pseudomonas syringae pv tomato* DC3000(*avrRpm1)* and incubated for 12 hours at RT. Leaves were then harvested and stained with Trypan Blue (*S8*) to visualize dead cells.

Conductivity measurements: three- or four-week-old-plants treated with the appropriate inducer of cell death (see Chemical Treatments) were harvested. If the leaves were big enough to be cored (Figs. 2A and 2B), leaf disks were removed (7 mm diameter), floated in water for 30 min and subsequently transferred to tubes containing 6 ml distilled water. If the plants were too small to be cored (Fig. 3C, Fig. 4A and Fig. S6B), whole leaves were harvested and their fresh weight determined. Plant material was then dipped into water to remove soil and subsequently transferred to tubes containing 6 ml distilled water. Conductivity of the solution was determined with an Orion Conductivity Meter at the indicated time points. Means and standard errors were calculated from four replicate measurements per genotype per experiment. For each measurement, we used six leaf disks or 40-50 mg fresh weight, which equaled 4-6 leaves. The entire experiment was performed three times.

Demonstration of lethality of *AtMC1-ΔN* in *lsd1*

We crossed *lsd1* (female) to two different *AtMC1-ΔN* overexpressing lines (1.3 and 2.8). F2 plants were selected for the presence of the transgene and analyzed for homozygosity of *lsd1*. Among 144 F2 individuals no homozygous *lsd1* plant was recovered.

Protein analysis

For the analysis of protein accumulation in Arabidopsis plants, leaf samples were snap frozen in liquid nitrogen and mechanically ground in 250 µl of plant extraction buffer (20 mM Tris, pH 7.5, 150 mM NaCl, 1mM EDTA, 1% Triton X-100 and 0.1% SDS) supplemented with a 1:100 dilution of plant protease inhibitor cocktail (Sigma-Aldrich). Protein extract was centrifuged 5 minutes at 10,000 *x g* at 4°C. The supernatants were collected, protein concentration was measured and the protein extracts were boiled on SDS-loading buffer (120 mM Tris, pH 6.8, 50% Glycerol, 6% SDS, 3 mM DTT and 1% Bromophenol blue) and separated on 12% SDS-PAGE gels. Proteins were transferred onto nitrocellulose membranes by semi-dry western blot. Membranes were first blocked with a 5% milk-Tris Buffer Saline-Tween 20 (TBST) solution and then incubated in a 1% milk-TBST solution containing a 1:5,000 dilution of anti-HA monoclonal antibody (3F10, Roche) or a 1:5 dilution of anti-myc monoclonal antibody (Tissue Culture Facility, UNC). Protein complexes were labeled with the appropriate horseradish peroxidase-conjugated secondary antibody (Santa Cruz Biotechnology) and detected using the Enhanced Chemiluminiscence Reagent (ECL), ECL-Plus or a 2:1 combination of ECL:ECL-Plus (GE Healthcare).

In order to analyze protein accumulation in yeast, EGY48 cells used for the yeast-two-hybrid assay (see below) were grown overnight in a 28°C shaker on 3 ml of selective Drop Out Base (DOB)-glucose selective media lacking tryptophan. The following day, OD_{600} was measured and adjusted to 0.2 in 4 ml of selective media. Cells were allowed to grow to an OD_{600} of 0.4 and were then centrifuged for 10 minutes at 10,000 x g. The pellets were resuspended in 100 µl of MURB buffer (50 mM Na_2HPO_4, 25 mM MES, pH 7, 3 M Urea, 1% SDS, 10% β-mercaptoethanol and 0.1% Bromophenol Blue) and processed into crude cell extracts by boiling. The extracts were subjected to immunoblot analysis as described above using anti-HA antisera.

Co-Immunoprecipation Assays

Whole *N. benthamiana* leaves (approx 1 g each) transiently expressing *Dex-AtMC1-HA* + *35S::p19* + empty vector filler (OD_{600} 0.2:0.2:0.8), *pLSD1::LSD1-myc* + *35S::p19* + empty vector filler (OD_{600} 0.8:0.2:0.2), *Dex-AtMC1-HA* + *pLSD1::LSD1-myc* + *35S::p19* (OD_{600} 0.2:0.8:0.2), *Dex-AtMC1-ΔN-HA* + *35S::p19* + empty vector filler (OD_{600} 0.2:0.2:0.8), *Dex-AtMC1-ΔN-HA* + *pLSD1::LSD1-myc* + *35S::p19* (OD_{600} 0.2:0.8:0.2), *Dex-AtMC2-HA* + *35S::p19* + empty vector filler (OD_{600} 0.2:0.2:0.8), *Dex-AtMC2-HA* + *pLSD1::LSD1-myc* + *35S::p19* (OD_{600} 0.2:0.8:0.2) and *Dex-AtMC1-HA* + *Est-AtMC2-myc* + *35S::p19* (OD_{600} 0.2:0.8:0.2) were frozen in liquid nitrogen. Samples were ground on ice in 3 ml co-immunoprecipitation extraction buffer (20 mM Tris-HCl pH 8, 150 mM NaCl, 100 µM $ZnSO_4$) supplemented with 1 mM DTT and 1:100 dilution of plant protease inhibitor cocktail (Sigma-Aldrich). Protein extracts were passed through a miracloth filter (Calbiochem) and centrifuged 15 minutes at 20,000 *x g* at 4°C. Supernatants were collected for further processing. Protein concentration was adjusted to 2 mg/ml. A 200 µl aliquot of this extract was immediately boiled in SDS-loading buffer (input). A second, 1 ml aliquot was incubated with anti-myc-conjugated magnetic beads (MACS) for 2 h at 4°C with constant rotation. The mixture was passed through a µ Column (MACS). Matrixes were first washed with Lysis Buffer (MACS), followed by three washes with co-immunoprecipitation extraction buffer before adding the bead/protein mix. Finally the columns were washed 4 times with extraction buffer (containing 250 mM NaCl and supplemented with 1 mM DTT) and then with Wash Buffer 2 (MACS) and the fraction of proteins bound to the beads were eluted with Elution Buffer (MACS) pre-heated to 95°C. 40 µg of input and 20 µl of eluate (16x concentrated compared to input) were separated on a SDS-PAGE gel and immunoblotted as described above.

Co-immunoprecipitation assays in Arabidopsis were performed with F1 plant populations originated from crosses between *lsd1 atmc1 pLSD1::LSD1-myc* and *lsd1 atmc1 Dex-AtMC1-HA transgenic lines. lsd1 atmc1 Dex-AtMC1-HA* plants were used as a negative control. The same protocol as described above for *N. benthamiana* was followed with the following changes: 200 mg of leaves were used per extraction; centrifugation was done at 4,000 x g; after adding the bead/protein mix, columns were washed three times with Wash Buffer 1 (MACS) adjusted to 300 mM NaCl; 65 µg of input was loaded on an SDS-PAGE gel when immunoblotted with anti-myc.

Pathogen Strains, Inoculation and Growth quantification

Hyaloperonospora arabidopsidis isolate Emwa1 and Noco2 were propagated on the susceptible Arabidopsis ecotypes Ws-2 and Col-0, respectively (*S14*). Conidiospores were suspended in water at a concentration of 50,000 spores/ml and spray-inoculated onto 11-16 day week old plants (*S9*). Inoculated plants were kept covered with a lid to increase humidity and grown at 19°C with a 9h light period. To test the growth of *Pseudomonas syringae pv. tomato* DC3000(*avrRpm1*) dip inoculations were performed as previously described (*S15, S16*).

Yeast-Two-Hybrid Analysis

Yeast-two-hybrid analysis was performed using the LexA system. Full length and deletion variants of AtMC1 and AtMC2 were cloned into a Gateway-compatible version of pEG202 (bait) and transformed into yeast RFY206 cells. Full length LSD1 and its deletion variants were cloned into a Gateway compatible version of pJG4-5 (prey) and transformed into yeast EGY48 cells. Mating was performed on 96-well plates overnight in a 28°C shaker. Colonies containing both plasmids were selected on Drop Out Base (DOB)-glucose selection media lacking uracil, tryptophan and histidine (-U, -W, -H). The interactions were analyzed qualitatively by re-streaking the yeast onto DOB-galactose (2%) /raffinose (1%) (-U, -W, -H) media containing 160 µg/ml of 5-bromo-4-chloro-3-indolyl β-D-galactopyranoside (X-Gal). The plates were incubated 1 or 2 days at 28ºC. As a negative control, DOB-glucose (-U, -W, -H) X-Gal plates were used. The interactions were considered positive if blue color developed on DOB-galactose/raffinose but not on DOB-glucose X-Gal plates. Quantitative β-Galactosidase colorimetric reporter activity assays were performed with a plate reader (Tecan) as described (S17).

Statistical analysis of data

Analysis of variance (ANOVA) was performed on the data, using the JMP program (SAS/JMP software; Version 7.0.1; SAS Institute). The Tukey's honestly significant difference (HSD) test ($P<0.05$) was applied to separate means.

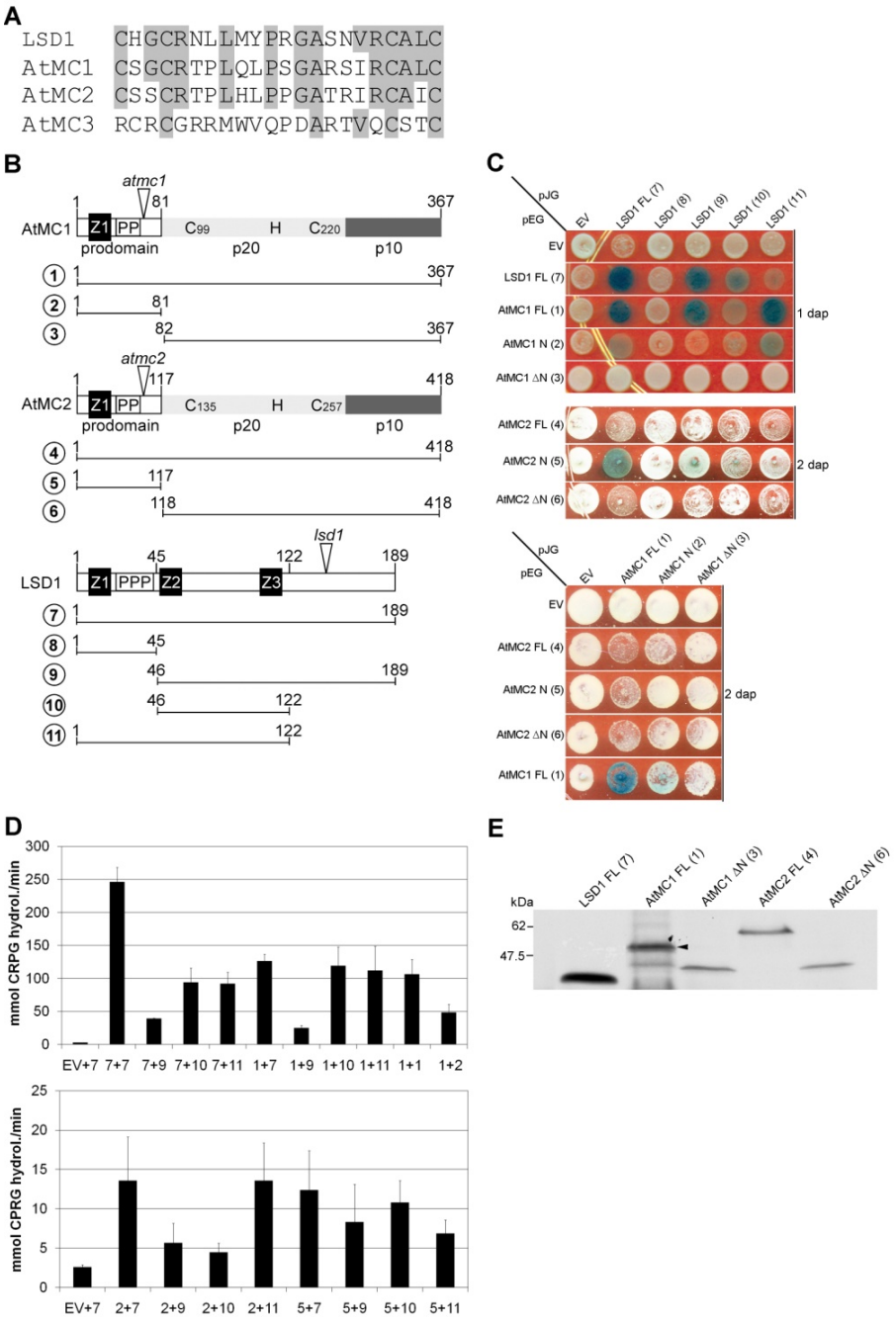

Figure S1: Yeast-two-hybrid analysis.

A) Sequence alignment of the CxxCRxxLMYxxGASxVxCxxC zinc-finger domain of LSD1 and the type I metacaspases AtMC1, AtMC2 and AtMC3 ("Z1" in **B)**). Note that the amino acid sequence of the AtMC3 Zinc finger domain is significantly divergent and AtMC3 was thus not considered in this work. **B)** Scheme of AtMC1, AtMC2 and LSD1 proteins (not to scale). Bars with numbers 1-11 inscribed in circles represent different fragments used for the yeast-two-hybrid assay; Z1, Z2 and Z3, LSD1-like zinc finger domains; PP and PPP, proline-rich region; p20 and p10, putative caspase-like catalytic domains; numbered H and C, putative catalytic

histidine and cysteines, present in the caspase-hemoglobinase fold (*S18*). *atmc1* and *atmc2* indicate the T-DNA insertion sites. **C)** Qualitative and **D)** quantitative analysis of the yeast-two-hybrid interactions between different combinations of AtMC1, AtMC2 and LSD1 shown in **(B)** where they are labeled 1-11. Pairwise interactions between LSD1 and AtMC1 and AtMC2 were tested using a LexA-based yeast-two-hybrid system. Full length LSD1 and its deletion variants (7-11 in **B)** were used as a prey. Full length AtMC1, or AtMC2 and their derivatives (1-6 in **B)** were used as bait. LSD1 can homodimerize in this assay (*S3*). **C)** Pictures of yeast growing on selective X-Gal media were taken 1 or 2 days after plating (dap). **D)** β-Galactosidase colorimetric reporter activity assays for quantitative analysis of the yeast-two-hybrid interactions. As expected, LSD1 interacted strongly with itself (246 ± 22 Miller units, mu). Moreover, LSD1 interacted with AtMC1 (126 ± 11 mu). Both the second and third zinc-fingers of LSD1 were required for the LSD1-AtMC1 interaction, but neither of them alone was sufficient. The same requirement was reported for the interaction between LSD1 and AtbZIP10, a transcription factor that acts antagonistically to LSD1 (*S3*). Interestingly, AtMC1 homodimerizes in this assay via its predicted prodomain (49 ± 12 mu). Both the predicted AtMC1 and AtMC2 prodomains interacted weakly (<15 mu), though above background, with full length LSD1 and truncated LSD1 derivatives containing the second and third zinc fingers. Conversely, the truncated forms of AtMC1 and AtMC2 lacking the predicted prodomain did not interact with each other or with any of the LSD1 variants (shown in **C)**. EV, empty vector. CPRG, Chlorophenol red-β-D-galactopyranoside substrate. Error bars represent 2x standard error. **E)** Proteins that do not interact in the yeast-two-hybrid assay are expressed in yeast (AtMC1-ΔN, AtMC2 and AtMC2-ΔN). Protein was extracted from EGY48 yeast cells and westerns were immunoblotted using the anti-HA antibody. The arrowhead indicates the band corresponding to AtMC1. Note that the proteins analyzed contain a translational fusion present in the pJG4-5 vector that increases their apparent molecular weight by 10.6 kDa.

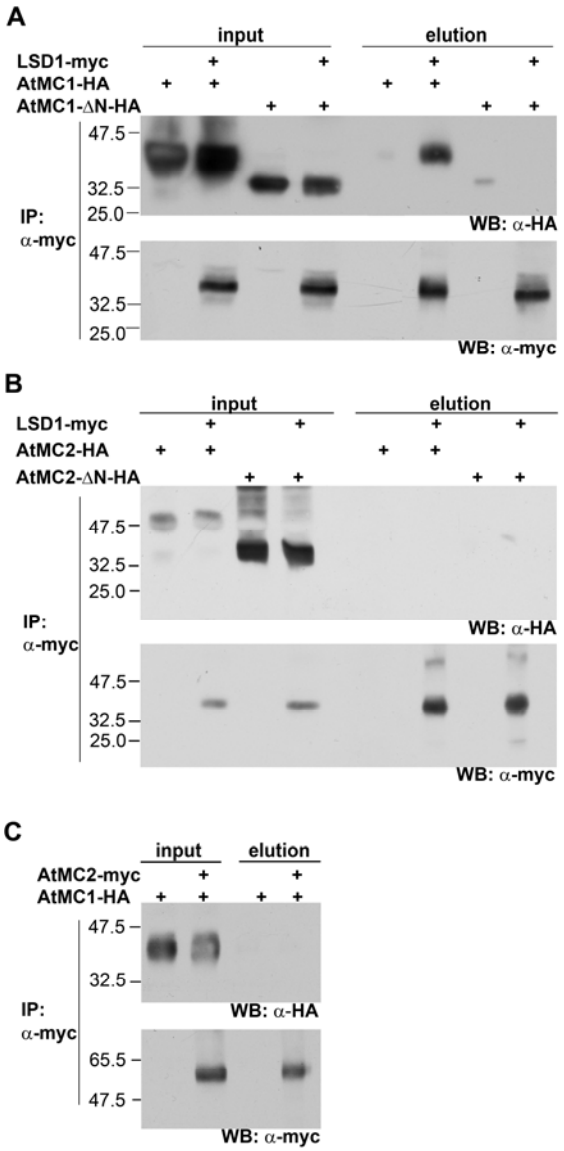

Figure S2: AtMC1 interacts with LSD1 via its putative prodomain. AtMC2 does not interact with LSD1 or AtMC1.

Protein extracts from *Nicotiana benthamiana* leaves transiently expressing **A)** full length *Dex-AtMC1-HA*, *Dex-AtMC1-ΔN-HA* lacking the putative prodomain or a mixture of *pLSD1::LSD1-myc* with either *Dex-AtMC1-HA* or *Dex-AtMC1-ΔN-HA*, **B)** *Dex-AtMC2-HA*, *Dex-AtMC2-ΔN-HA* or a mixture of *pLSD1::LSD1-myc* with either *Dex-AtMC2-HA* or *Dex-AtMC2-ΔN-HA* and **C)** *Dex-AtMC1-HA* or a mixture of *Dex-AtMC1-HA* with *Est-AtMC2-myc*, were subjected to immunoprecipitation using anti-myc-coupled magnetic beads. Forty μg of crude extract (input) and a 16x concentrated fraction containing the eluate (elution) were analyzed by SDS-PAGE/anti-HA or anti-myc immunoblot.

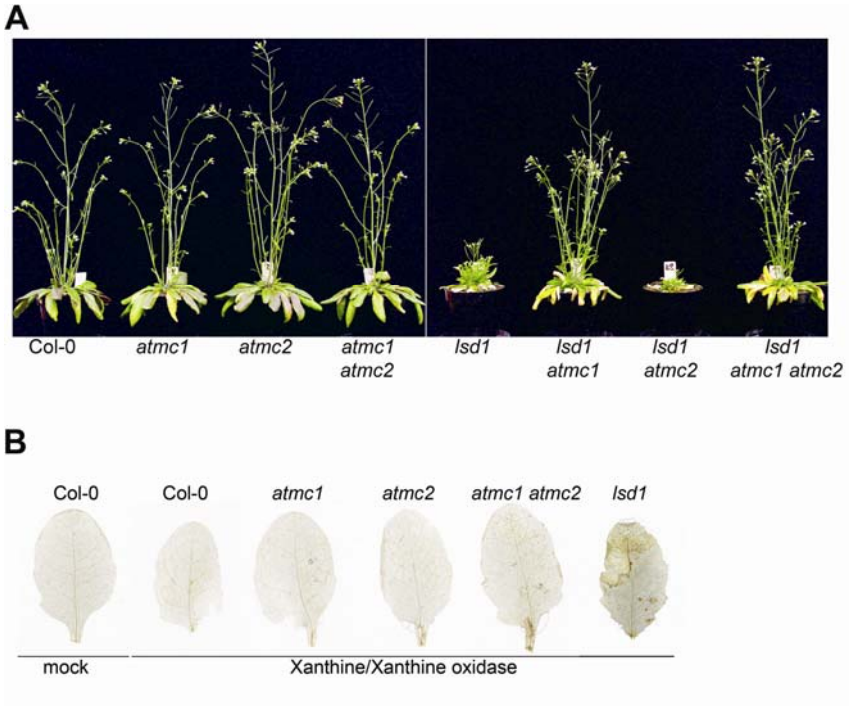

Figure S3: Developmental and stress-related phenotypes.

A) Pictures of eight-week-old Col-0 wild type and the mutants used in this study. Plants were grown in a growth chamber under short-day conditions during 15 days and then transferred to the greenhouse and grown under long-day conditions for 6 more weeks. **B)** 3,3'-Diaminobenzidine (DAB) stains of leaves from 4-week-old Col-0 and the mutants used in this study 3 days after infiltration with Xanthine/Xanthine Oxidase (X/XO).

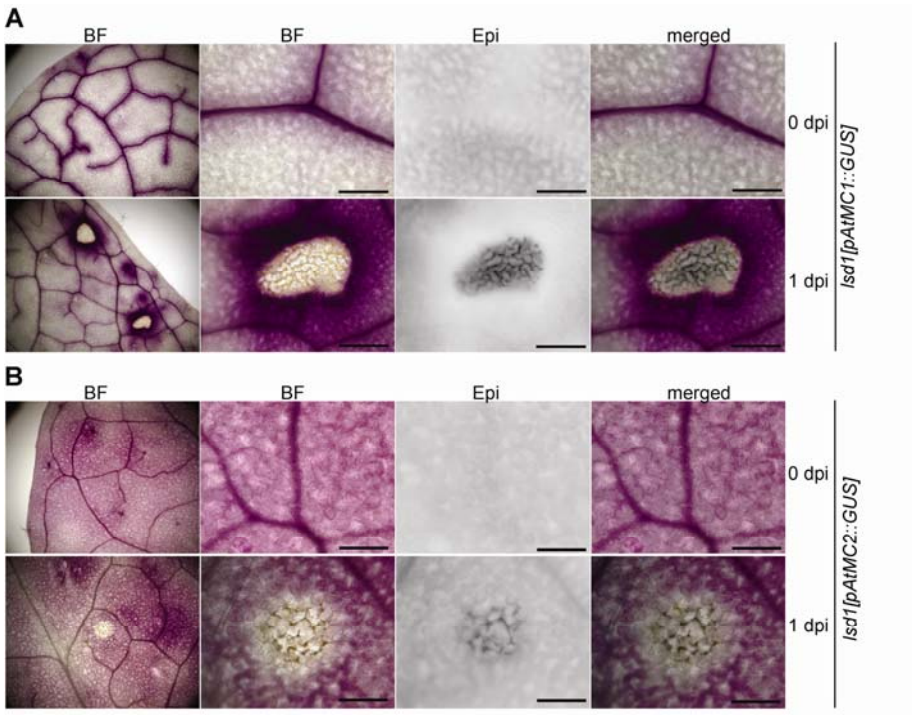

Figure S4: AtMC1 is expressed in spatially restricted zones at *lsd1* runaway cell death sites.

Four-week-old plants of the genoptypes *lsd1[pAtMC1::GUS]* **(A)** and *lsd1[pAtMC2::GUS]* **(B)** were sprayed with 150 µM BTH. Leaves were harvested at 0 and 1 day after treatment (dpi), stained with Magenta-Gluc and analyzed under bright field and UV-epifluorescence to detect induction of expression and auto-fluorescent secondary metabolites that accumulate upon cell death (*S19*), respectively. Scalebar, 100 µm; BF, bright field; Epi, epifluorescence, inverted; merged, BF and Epi pictures merged.

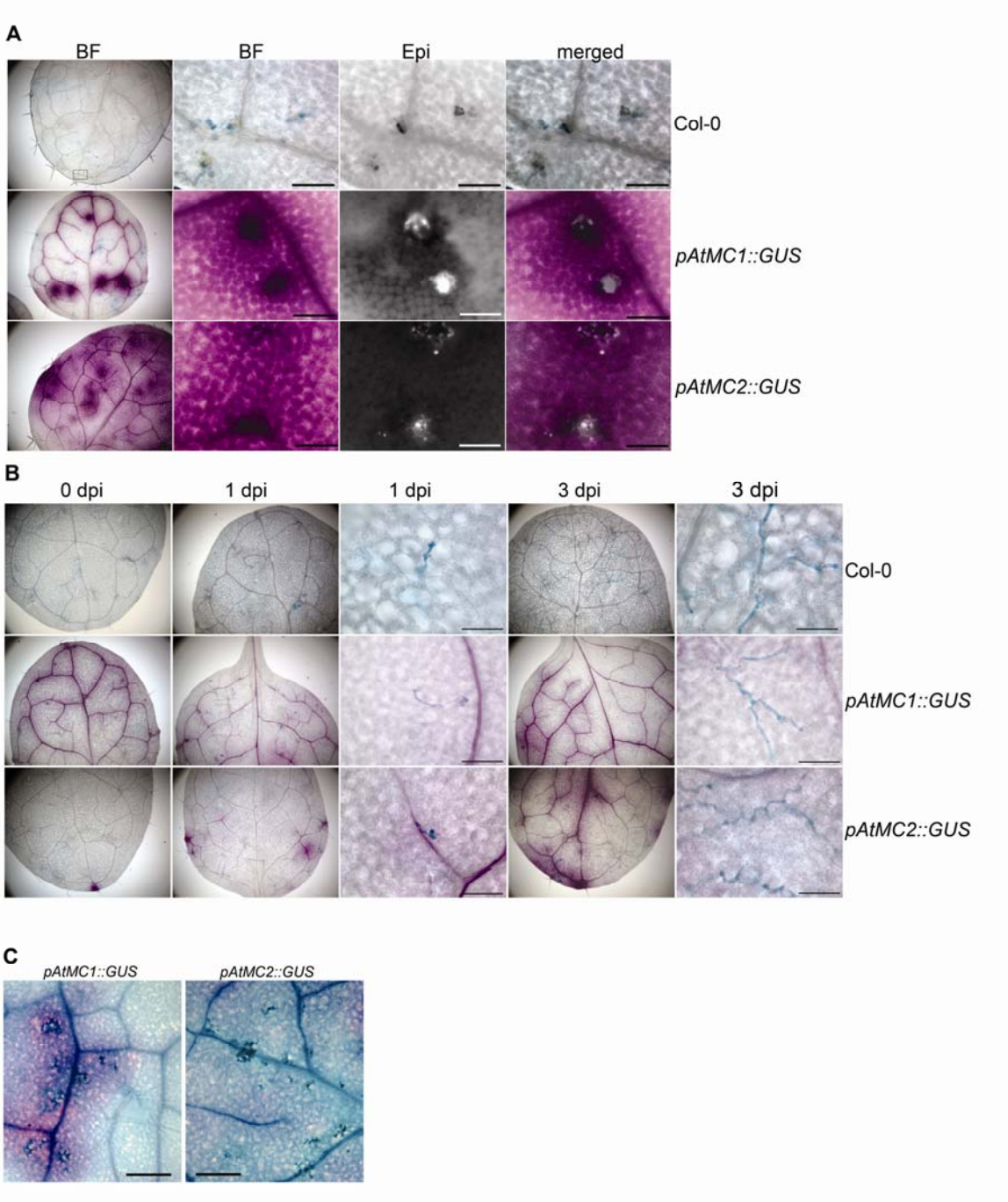

Figure S5: *AtMC1* is expressed in spatially restricted zones at HR sites

A) Two-week-old Col-0, *pAtMC1::GUS* or *pAtMC2::GUS* plants were inoculated with 50,000 spores/ml of the *Hpa* isolate Emwa1 to trigger RPP4-mediated HR and disease resistance. At 2 dpi, primary leaves were harvested and double stained with Magenta-Gluc and Aniline Blue, which stains callose deposits and is a proxy for HR (*S11, S19*). Epifluorescence was used to visualize aniline blue stained callose deposition and *Hpa* hyphae. Scalebar, 100 μm; BF, bright field; Epi, epifluorescence (inverted for Col-0); merged, BF and Epi pictures merged. As

expected, infected Col-0 exhibited HR at sites of autoflourescence (top row). *pAtMC1::GUS* plants displayed intense Magenta-Gluc staining in a limited spatial zone of several cells directly surrounding HR sites (middle row). *pAtMC2*-driven GUS-expression was also present around infection sites, but was spatially more diffuse than that of *pAtMC1::GUS* (lower row). **B)** Two-week-old Col-0, *pAtMC1::GUS* or *pAtMC2::GUS* plants were inoculated with 50,000 spores/ml of the virulent *Hpa* isolate Noco2. At 1 and 3 dpi, primary leaves were harvested and double stained with Magenta-Gluc and Aniline Blue. Scalebar, 100 μm. There is no induced expression of *AtMC1* around the freely elongating hyphae (blue stained) (middle row), nor does this pathogen isolate alter the weak expression of *AtMC2* (bottom row). **C)** *AtMC1* expression is induced after inoculation with hemibiotrophic *Pseudomonas syringae* pv. *tomato* strain DC3000(*avrRpm1*) to trigger RPM1-mediated HR and disease resistance. 16-day-old *pAtMC1::GUS* or *pAtMC2::GUS* plants were vacuum infiltrated with 500,000 cfu/ml of *Pto* DC3000(*avrRpm1*). Primary and secondary leaves were harvested 12 hours later and double stained with Magenta-Gluc and Trypan Blue. Scalebar, 200 μm. *AtMC1* was expressed adjacent to HR sites following recognition *Pto* DC3000(*avrRpm1*) (left). *AtMC2* expression was diffuse and excluded from HR sites (right).

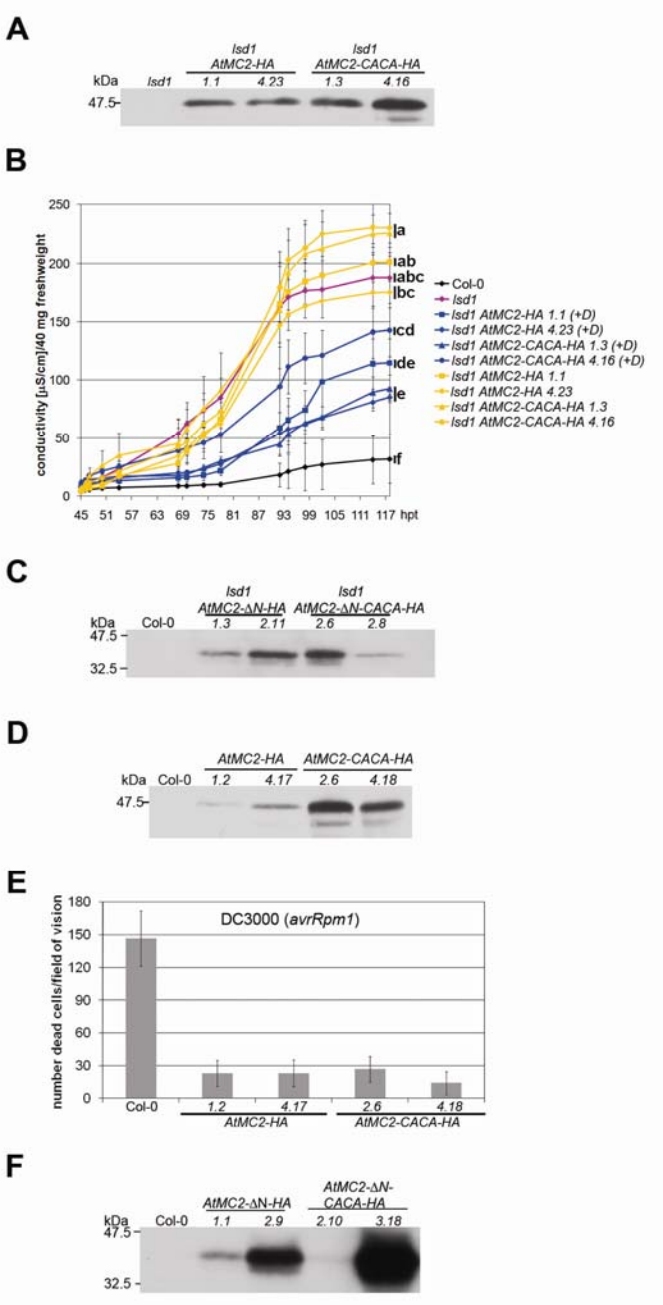

Figure S6: Full-length AtMC2 is a negative regulator of cell death.

Seedlings of the depicted genotypes were sprayed with 1 μM Dex 6, 11 and 16 days after germination. CACA, denotes constructs where both putative catalytically active cysteine residues (C135A C256A) have been mutated to alanine. **A, C, D and F)** AtMC2 protein accumulation in different transgenic lines. One day after the last treatment with Dex, tissue was harvested and total protein isolated. Westerns were immunoblotted with the anti-HA antibody**. B)** Full-length *AtMC2* partially inhibits *lsd1* runaway cell death. One day after the last treatment with Dex, plants were sprayed with 150 μM BTH. Tissue was harvested at 43 hpt and processed

for conductivity measurements. Blue lines: Dex-treated genotypes; Yellow lines: non Dex-treated genotypes. Error bars represent 2 x standard error. Letters a - f represent experimental groups with significant differences (P <0.05, Tukey's HSD test). The experiment was repeated twice. hpt, hours after treatment. **E)** Ten hours after the last treatment with Dex plants were vacuum infiltrated with 500,000 cfu/ml of *Pto* DC3000(*avrRpm1*). Twelve hours later, plants were harvested and stained with Trypan Blue to visualize cell death. To quantify cell death, all dead cells in one field of vision (10x magnification) were counted. Average and 2 x standard error were calculated from 20 leaves per genotype and treatment.

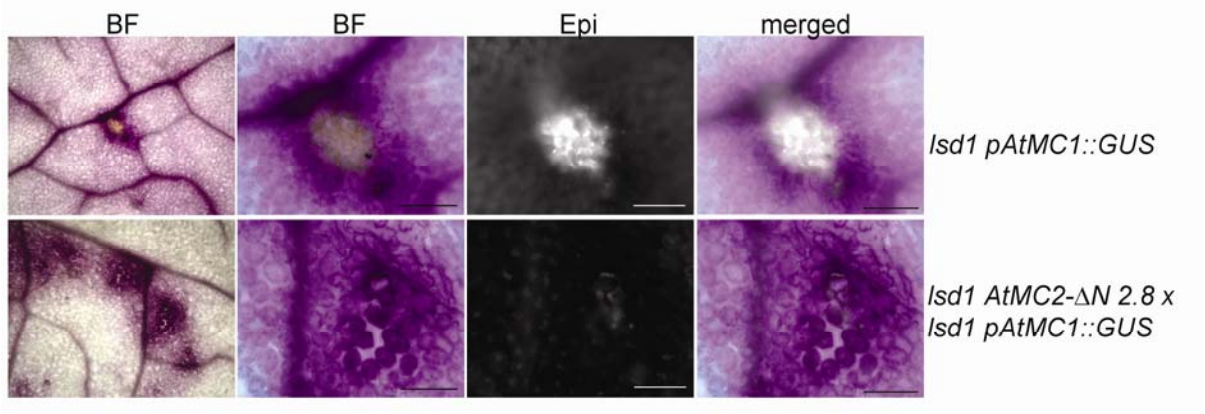

Figure S7: AtMC2 does not transcriptionally regulate AtMC1

An *lsd1 pAtMC1::GUS* line was crossed to *lsd1 AtMC2-ΔN* line 2.8. F1 seedlings and seedlings of the *lsd1 pAtMC1::GUS* parental control line were treated with 1 μM Dex 6, 11 and 16 days after germination. One day after the last treatment with Dex, plants were treated with 150 μM BTH. Leaves were harvested 1 day after BTH treatment, stained with Magenta-Gluc and analyzed under bright field and UV-epifluorescence to detect induction of AtMC1 expression and auto-fluorescent secondary metabolites that accumulate upon cell death (*S19*), respectively. Scalebar, 100 μm; BF, bright field; Epi, epifluorescence; merged, BF and Epi pictures merged. Note the suppression of autofluorescence, but not Magenta-Gluc staining in samples from the F1, confirming that although *pAtMC1::GUS* is still expressed, the wild type AtMC1 activity is suppressed.

References for SOM

S1. J. M. Alonso *et al.*, *Science* **301**, 653 (2003).
S2. T. Aoyama, N. H. Chua, *Plant J* **11**, 605 (1997).
S3. H. Kaminaka *et al.*, *EMBO J* **25**, 4400 (2006).
S4. T. Nakagawa *et al.*, *J Biosci Bioeng* **104**, 34 (2007).
S5. M. D. Curtis, U. Grossniklaus, *Plant Physiol* **133**, 462 (2003).
S6. O. Voinnet, S. Rivas, P. Mestre, D. Baulcombe, *Plant J* **33**, 949 (2003).
S7. S. J. Clough, A. F. Bent, *Plant J* **16**, 735 (Dec, 1998).
S8. R. C. Keogh, B. J. Deverall, S. McLeod, *Transactions of the British Mycological Society* **74**, 329 (1980).
S9. E. Koch, A. Slusarenko, *Plant Cell* **2**, 437 (1990).
S10. R. A. Dietrich, M. H. Richberg, R. Schmidt, C. Dean, J. L. Dangl, *Cell* **88**, 685 (1997).
S11. W. Eschrich, H. B. Currier, *Stain Technology* **39**, 303 (1964).
S12. M. A. Torres, J. L. Dangl, J. D. Jones, *Proc Natl Acad Sci U S A* **99**, 517 (2002).
S13. N. Hatsugai *et al.*, *Genes Dev* **23**, 2469 (2009).
S14. N. H. Chua, C. Koncz, J. S. Schell, *Methods in Arabidopsis research*. (World Scientific, Singapore ; River Edge, N.J., 1992).
S15. T. K. Eitas, Z. L. Nimchuk, J. L. Dangl, *Proc Natl Acad Sci U S A* **105**, 6475 (2008).
S16. P. Tornero, J. L. Dangl, *Plant J* **28**, 475 (2001).
S17. I. G. Serebriiskii, G. G. Toby, E. A. Golemis, *Biotechniques* **29**, 278 (2000).
S18. A. G. Uren *et al.*, *Mol Cell* **6**, 961 (2000).
S19. R. A. Dietrich *et al.*, *Cell* **77**, 565 (1994).